

# First Glimpses at Higgs' face

J.R. Espinosa,<sup>1</sup> C. Grojean,<sup>2</sup> M. Mühlleitner,<sup>3</sup> and M. Trott<sup>2</sup>

<sup>1</sup>*ICREA at IFAE, Universitat Autònoma de Barcelona, 08193 Bellaterra, Barcelona, Spain*

<sup>2</sup>*Theory Division, Physics Department, CERN, CH-1211 Geneva 23, Switzerland*

<sup>3</sup>*Institute for Theoretical Physics, Karlsruhe Institute of Technology, D-76128 Karlsruhe, Germany*

(Dated: July 17, 2022)

The 8 TeV LHC Higgs search data just released indicates the existence of a scalar resonance with mass  $\sim 125$  GeV. We examine the implications of the data reported by ATLAS, CMS and the Tevatron collaborations on understanding the properties of this scalar by performing joint fits on its couplings to other Standard Model particles. We discuss and characterize to what degree this resonance has the properties of the Standard Model (SM) Higgs, and consider what implications can be extracted for New Physics in a (mostly) model-independent fashion. We find that, if the Higgs couplings to fermions and weak vector bosons are allowed to differ from their standard values, the SM is  $\sim 2\sigma$  from the best fit point to current data. Fitting to a possible invisible decay branching ratio, we find  $\text{BR}_{\text{inv}} \simeq 0.05 \pm 0.32$  (95% C.L.) We also discuss and develop some ways of using the data in order to bound or rule out models which modify significantly the properties of this scalar resonance and apply these techniques to the global current data set.

## I. INTRODUCTION

Particle physics entered a new era with the announcement of the discovery of a new boson [1] based on excess events in several Higgs search channels using 7 + 8 TeV LHC data collected in 2011-2012. In light of this discovery, it has become obvious that the question of central importance to address now is – what are the properties of the scalar field responsible for the observed excesses? Answering this question allows us to determine if this field corresponds to the Standard Model (SM) Higgs, with the specific SM mechanism of elegantly breaking electroweak (EW) symmetry, or whether a more complicated mechanism is involved in EW symmetry breaking. We study this question in detail in this paper, characterizing to what degree a SM Higgs is consistent with the current global data set and presenting several results on the properties of the scalar field. Besides

updating and expanding our past results [2], we also present new analyses that emphasize the power of the growing dataset to bound and rule out alternative models or to give hints of New Physics (NP).

It is worth emphasizing that it is very important to specify (and justify) a coherent theoretical framework in which to study the emerging evidence for the scalar field. However, without knowing the ultraviolet (UV) origin of this field, we do not know what effective field theory (EFT), or complete model, should be used to fit the data. We emphasize that at this time, the existing experimental evidence is not sufficiently strong to directly assume that the scalar resonance is the SM Higgs boson, ascribing any deviations in the measured properties of the scalar field directly to the effects of NP interactions expressed through higher dimensional operators. Although this is certainly one possible interpretation of the data (and we will examine the implications of Higgs data for NP in this framework), we emphasize that, in general, one should not assume what one wishes to prove.

Nevertheless, in formulating a theoretical framework for this study, a wealth of other experimental results that are also sensitive to the properties of scalar fields at the weak scale can be distilled into simple physical principles. These are, namely, approximate Minimal Flavour Violation (MFV) [3–7], respecting the soft Higgs theorems of Refs. [8, 9] (i.e. the scalar couples to the SM fields in proportion to their masses), and an effective breaking of custodial symmetry,  $SU(2)_c$ , [10–12] approximately as in the SM. Directly incorporating these principles to guide the formulation of the effective Lagrangian allows us to restrict our attention to a few simple cases. In order to establish experimentally the properties of the scalar resonance in a model-independent way, one can utilize the effective field theory of the chiral EW Lagrangian coupled to a scalar field that was emphasized in [2, 13] to study recent Higgs signal-strength data.<sup>1</sup> Depending on the assumptions of the UV origin of such a Lagrangian, one is lead to various sets of free parameters to fit the data with when studying the consistency of the SM Higgs hypothesis with the current data set. We discuss and utilize this framework extensively in this paper when examining the properties of the scalar field emerging from the data.

We also emphasize that with the discovery of a new scalar resonance, one can also use the signal strength properties of the scalar field to bound and rule out models that provide *too few* signal events as well as models that provide too many signal events. Further, one can also exclude allowed

---

<sup>1</sup> For other model-independent approaches to the determination of the Higgs couplings, see [14–22].

parameter space due to the degree of tension within the data set that depends on the properties of the scalar field. As the data set evolves these techniques become complementary to direct  $\chi^2$  fits on the signal strength data set. These bounds can be quantified by excluding parameter space in the allowed couplings of the scalar using a gaussian probability density function approach. We develop and apply such an approach in this paper.

The outline of this paper is as follows. In Section II we discuss the EFT approach we employ, and the implicit assumptions about the UV origin of the scalar field that are adopted when fitting the data with various free parameters. In Section III we review and discuss the manner in which we treat the scalar signal strength data and electroweak precision data (EWPD), in Section IV we present results, based on our fit method, of the status of the SM Higgs hypothesis. In Section IV B we discuss some of the implications of Higgs signal strength parameters for beyond the SM (BSM) physics expressed through model-independent free parameters. In Section V we discuss novel and complementary methods to examine the allowed parameter space, and in Section VI we conclude.

## II. THEORETICAL FRAMEWORK

A minimal description of the (non-scalar) degrees of freedom of the SM consistent with the assumptions of SM-like  $SU(2)_c$  violation, that can also be consistent with MFV, and respects the soft Higgs theorems, is given by an effective chiral EW Lagrangian with a nonlinear realization of the  $SU(2)_L \times U(1)_Y$  symmetry. The Goldstone bosons eaten by the  $W^\pm, Z$  are denoted by  $\pi^a$  (where  $a = 1, 2, 3$ ), and are grouped as

$$\Sigma(x) = e^{i\sigma_a \pi^a/v}, \quad (1)$$

with  $\sigma_a$  the Pauli matrices and  $v = 246 \text{ GeV}$ .

In this approach, the EW scale  $v$ , which sets the mass of fermions and gauge bosons is introduced directly into the Lagrangian. The  $\Sigma(x)$  field transforms linearly under  $SU(2)_L \times SU(2)_R$  as  $\Sigma(x) \rightarrow L \Sigma(x) R^\dagger$  where  $L, R$  indicate the transformation on the left and right under  $SU(2)_L$  and  $SU(2)_R$ , respectively, while  $SU(2)_c$  is the diagonal subgroup of  $SU(2)_L \times SU(2)_R$ .

Adding a scalar field  $h$  to this theory is trivial. One choses  $h$  to transform as a singlet under

$SU(2)_c$  and a derivative expansion of such a theory is given by [23–25]

$$\begin{aligned} \mathcal{L}_{eff} = & \frac{1}{2}(\partial_\mu h)^2 - V(h) + \frac{v^2}{4}\text{Tr}(D_\mu \Sigma^\dagger D^\mu \Sigma) \left[ 1 + 2a \frac{h}{v} + b \frac{h^2}{v^2} + b_3 \frac{h^3}{v^3} + \dots \right], \\ & - \frac{v}{\sqrt{2}} (\bar{u}_L^i \bar{d}_L^j) \Sigma \left[ 1 + c_j \frac{h}{v} + c_2 \frac{h^2}{v^2} + \dots \right] \begin{pmatrix} y_{ij}^u u_R^j \\ y_{ij}^d d_R^j \end{pmatrix} + h.c. \dots, \end{aligned} \quad (2)$$

with

$$V(h) = \frac{1}{2} m_h^2 h^2 + \frac{d_3}{6} \left( \frac{3 m_h^2}{v} \right) h^3 + \frac{d_4}{24} \left( \frac{3 m_h^2}{v^2} \right) h^4 + \dots \quad (3)$$

Although we use the notation  $h$ , we do not assume that this scalar field is the Higgs, or that the scale  $v$  is somehow associated with the vacuum expectation value of this field – as this is what we seek to establish from the data. As is well known, the  $a$  and  $c_j$  parameters control the couplings of  $h$  to gauge bosons and fermions, respectively, and therefore, play a crucial role in the phenomenology of single  $h$  production. Note that in previous fits, and in the majority of this work, the assumption  $c_j y_{ij}^{u,d} \equiv c y_{ij}^{u,d}$  is used and no distinction is made between the rescaling of the  $h$ -coupling to the  $u$  and  $d$  quarks. We will relax this assumption later on. This Lagrangian is common in the study of composite models and has been emphasized recently in Refs. [23–25]. It is also appropriate to study a pseudo-Goldstone boson (PGB) emerging out of an approximately conformal sector [26, 27], or as the low-energy EFT arising in many scenarios where the Higgs is a composite PGB that emerges from the breaking of a larger chiral symmetry group [28–31]. We emphasize that this EFT setup can be matched to many UV frameworks and, being quite general, we do not confine ourselves to any particular UV scenario.<sup>2</sup>

We approach the data in this way to be as model-independent as possible. However, even specifying the free parameters that one will use to fit the data introduces implicit model dependence. One can nevertheless broadly characterize certain parameter choices. As this is an EFT,  $\mathcal{L}_{eff}$  is non-renormalizable. Since we are concerned with the phenomenology of single scalar production, the higher-order derivative operators are suppressed by powers of  $\mathcal{O}(m_h^2/(16\pi^2 v^2 (1-a^2)))$ . Here (and throughout this paper) we take the cut-off scale to be  $\Lambda \sim 4\pi v \sqrt{1-a^2}$ . As such, we are justified in neglecting such sub-leading effects in this paper. Non-derivative higher-dimensional

---

<sup>2</sup> The symmetry assumptions we adopt by directly interpreting the data are minimal. In more involved scenarios, these assumptions can in principle be relaxed (see *e.g.* Ref. [32] for a study with this aim that relaxes  $SU(2)_c$  constraints). Note, however, that relaxing the assumption  $c_j y_{ij}^{u,d} \equiv c y_{ij}^{u,d}$  significantly can lead to conflict with precision constraints sensitive to  $SU(2)_c$  and flavour violation.

operators, however, also exist. When the  $h$  field is not assumed to have a UV origin such as the SM Higgs, and is simply considered to be a singlet field (that need not necessarily transform under the nonlinearly realized  $SU(2)_L \times U(1)$  symmetry), the leading operators in the expansion in inverse powers of  $\Lambda$  appear at dimension five and are given by

$$\mathcal{L}_{HD}^5 = -\frac{c_g g_3^2}{2\Lambda} h G_{\mu\nu}^A G^{A\mu\nu} - \frac{c_W g_2^2}{2\Lambda} h W_{\mu\nu}^a W^{a\mu\nu} - \frac{c_B g_1^2}{2\Lambda} h B_{\mu\nu} B^{\mu\nu}. \quad (4)$$

Here  $g_1, g_2, g_3$  are the weak hypercharge,  $SU(2)_L$  gauge and  $SU(3)$  gauge couplings, respectively, and the different tensor fields are the corresponding field strengths with their associated Wilson coefficients  $c_i$ . The scale  $\Lambda$  corresponds to the mass scale of the lightest new state that is integrated out, which we assume is proximate to  $\Lambda$ . We will neglect operators originating from CP-violating sources due to the lack of any clear evidence of beyond the SM (BSM) CP violation in lower energy precision tests. Note that the operators in  $\mathcal{L}_{HD}^5$  can be further suppressed compared to the effects of  $a, c$  on (single) scalar production when the scalar field has specific UV origins. This is the case for example when  $h$  is a PGB, see Ref. [23] for a detailed discussion.

When one assumes that  $h$  is embedded into an  $SU(2)_L$  doublet -  $H$  - as in the SM, the operators in  $\mathcal{L}_{HD}^5$  first appear at dimension six, and the coefficients are suppressed by an extra factor of  $v/\Lambda$  when considering single scalar production. In this case, the dimension six operator basis is also extended by the operator

$$\delta\mathcal{L}_{HD}^6 = -\frac{c_{WB} g_1 g_2}{2\Lambda^2} H^\dagger \tau^a H B_{\mu\nu} W^{a\mu\nu}. \quad (5)$$

For phenomenological purposes it is convenient to rotate to a basis for the operators given by

$$\mathcal{L}_{HD} = -\frac{c_g g_3^2}{2\Lambda} h G_{\mu\nu}^A G^{A\mu\nu} - \frac{c_\gamma (2\pi\alpha)}{\Lambda} h F_{\mu\nu} F^{\mu\nu}, \quad (6)$$

where  $F_{\mu\nu}$  is the electromagnetic field strength tensor and  $c_\gamma = c_W + c_B$  in the case of an  $SU(2)_L$  singlet field, and  $c_\gamma = c_W + c_B - c_{WB}$  if  $h$  is embedded into an  $SU(2)_L$  doublet.

In this manner, one can understand that the choices to retain the effects of higher dimensional operators (or not) in performing global fits introduces implicit UV dependence. In introducing higher dimensional operators, one is also explicitly assuming the existence of new states charged under at least a subgroup of the SM group. Alternatively, if NP is uncharged under the SM group but couples to the  $h^2$  operator, then it can impact  $h$ -phenomenology by inducing an invisible  $h$ -width (when the scalar field takes on a vacuum expectation value). This leads to the modification of the SM branching ratios for each decay into visible SM final states  $f$  via

$$\text{Br}(h \rightarrow f) \equiv (1 - \text{Br}_{inv}) \times \text{Br}_{SM}(h \rightarrow f). \quad (7)$$

New physics of this form is sometimes referred to as coupling to the SM through the Higgs portal, see Refs. [33–37] for some related discussion. We will update our recent fit [38] for the parameter  $\text{Br}_{inv}$  in a later section, and use this fit as a diagnostic tool to test aspects of our fit procedure. In general, the coefficients  $a, c, c_\gamma, c_g, \text{Br}_{inv} \dots$  are arbitrary parameters subject to experimental constraints. The cases that we will consider in detail are:

- Composite/Pseudo-Goldstone Higgs/Dilaton scalar theories.
  - In this case,  $a, c$  are free parameters in general, although they can be fixed in particular UV completions. If the scalar field is a Pseudo-Goldstone boson, it is also appropriate to neglect higher dimensional operators. We will fit to subsets of the parameters  $\{a, c, \text{Br}_{inv}, c_\gamma, c_g\}$  in what follows. As this is a more general framework than the SM Higgs, we will use this EFT in assessing to what degree the SM Higgs hypothesis is consistent with the data.
- The SM Higgs as a low-energy EFT.
  - When the low-energy EFT is just the SM, the field  $h$  becomes part of a linear multiplet

$$U = \left(1 + \frac{h}{v}\right) \Sigma, \quad (8)$$

reducing Eq. (2) to the SM Higgs Lagrangian. In this case  $a = b = c = d_3 = d_4 = 1$  and  $b_3 = c_2 = 0$ , and the only effect of NP is through non-renormalizable higher-order operators. The naturalness problem of the SM Higgs mass operator, and recent experimental hints for deviations in the observed properties of the (assumed) Higgs, motivates moderately heavy NP and the introduction of BSM parameters ( $c_\gamma, c_g, \text{Br}_{inv}$ ) as free parameters. We study the constraints on these parameters in detail in this paper.

We will not attempt to relate the constraints obtained on the various parameters to any particular underlying model, other than the SM, in this paper. This choice is motivated by the current lack of other clear experimental evidence of BSM states to guide coherent model-building. The classes of models discussed above can be considered as motivating examples.

### III. DATA TREATMENT

#### A. Signal-Strength Data

In this section we describe our method for globally fitting to the parameters discussed above, and incorporating the recently released 8 TeV data [1], updated 7 TeV results from ATLAS [39], the released 7 TeV CMS data [40], and the recently reported Tevatron Higgs search results [41]. This work builds on our previous fits [2, 38]. We only summarize the main details of the fit procedure and method here. Many subsidiary details of the fit procedure we relegate to these reference works.

We fit to the available Higgs signal strength data,

$$\mu_i = \frac{[\sum_j \sigma_{j \rightarrow h} \times \text{Br}(h \rightarrow i)]_{\text{observed}}}{[\sum_j \sigma_{j \rightarrow h} \times \text{Br}(h \rightarrow i)]_{SM}}, \quad (9)$$

for the production of a Higgs that decays into the visible channels  $i = 1 \cdots N_{ch}$ , where  $N_{ch}$  denotes the number of channels. The label  $j$  in the cross section,  $\sigma_{j \rightarrow h}$ , is due to the fact that some final states are defined to only be summed over a subset of Higgs production processes  $j$ . The reported best-fit value of a signal strength we denote by  $\hat{\mu}_i$ .

The global  $\chi^2$  we construct is defined via

$$\chi^2(\mu_i) = \sum_{i=1}^{N_{ch}} \frac{(\mu_i - \hat{\mu}_i)^2}{\sigma_i^2}. \quad (10)$$

The covariance matrix has been taken to be diagonal with the square of the  $1\sigma$  theory and experimental errors added in quadrature for each observable, giving the error  $\sigma_i$  in the equation above. Correlation coefficients are neglected as they are not supplied by the experimental collaborations. For the experimental errors we use  $\pm$  symmetric  $1\sigma$  errors on the reported  $\hat{\mu}_i$ . For theory predictions of the  $\sigma_{j \rightarrow h}$  and related errors, we use the numbers given on the webpage of the LHC Higgs Cross Section Working Group [42].<sup>3</sup> The minimum ( $\chi_{min}^2$ ) is determined, and the 68.2% ( $1\sigma$ ), 95% ( $2\sigma$ ), 99% ( $3\sigma$ ) best fit regions are plotted as  $\chi^2 = \chi_{min}^2 + \Delta\chi^2$ , with the appropriate cumulative distribution function (CDF) defining  $\Delta\chi^2$ .

---

<sup>3</sup> These values have recently been updated for 7, 8 TeV and we use the updated numbers. Also note that  $\text{BR}(s\bar{s})$  is set to zero on this page but we use the latest version of HDECAY [43] to add in  $\text{BR}(s\bar{s})$  to the quoted results. This has a negligible impact on the reported numbers through the modification of the total width.

We assume, as in Ref. [2, 13], that the signal strength  $\mu$  in the considered channels  $i$  follows a Gaussian distribution with the probability density function (pdf) given by

$$\text{pdf}_i(\mu_i, \hat{\mu}_i, \sigma_i) \approx e^{-(\mu - \hat{\mu}_i)^2 / (2\sigma_i^2)}, \quad (11)$$

with the one-sigma error  $\sigma_i$ , and the best-fit value  $\hat{\mu}_i$ . This is the case as long as the number of events is large,  $\gtrsim \mathcal{O}(10)$  events, [13]. We normalize these pdf's to 1 in the interval  $(0, \infty)$ .

By multiplying together all the individual channel pdf's, or the pdf's of a single channel reported at two operating energies, we can also define a combined PDF. This can be done for each separate experiment or for a global combination of all experiments. The combined PDF is also Gaussian and has combined  $\hat{\mu}_c$  and  $\sigma_c$  values given approximately<sup>4</sup> by

$$\frac{1}{\sigma_c^2} = \sum_i^{N_{ch}} \frac{1}{\sigma_i^2}, \quad \hat{\mu}_c = \sum_i^{N_{ch}} \frac{\hat{\mu}_i}{\sigma_i^2}. \quad (12)$$

We will use these relations to reconstruct the unreported 8 TeV data from the reported 7 and 7 + 8 TeV data. See the Appendix for more details. Note that such combined parameters for the full dataset are directly related to our  $\chi^2$  measure by the relation

$$\chi^2(\mu) = \frac{1}{\sigma_c^2} (\mu - \mu_c)^2 + \left[ \sum_{i=1}^{N_{ch}} \frac{\mu_i^2}{\sigma_i^2} - \frac{\hat{\mu}^2}{\sigma_c^2} \right]. \quad (13)$$

Armed with a  $\chi^2$  measure or such combined PDF(s), we can determine the 95% C.L. exclusion upper limits on the signal strength parameter  $\mu$  ( $\mu < \mu_{upL}$ ) [2, 13]. With  $\hat{\mu}_i$ 's settling around unity with  $\sigma_i$  errors getting smaller and smaller due to increasing integrated luminosities, we can already start to set also *lower* limits on  $\mu$ . The condition for such lower bounds, say at 95% C.L., to be meaningful is that the symmetric interval  $\hat{\mu} \pm \delta_{95}\hat{\mu}$  containing 95% of the integrated probability has  $\hat{\mu} - \delta_{95}\hat{\mu} > 0$ , in which case  $\mu_{dwL} \equiv \hat{\mu} - \delta_{95}\hat{\mu}$  corresponds to the lower 95% C.L. bound on  $\mu$ . In this same case, we will take  $\hat{\mu} + \delta_{95}\hat{\mu} > 0$  as the upper limit  $\mu_{upL}$ . The conditions that define these limit are therefore

$$\int_{\mu_{dwL}}^{\hat{\mu}} \text{PDF}(\mu) d\mu = \frac{\text{Erf} \left[ \frac{\hat{\mu} - \mu_{dwL}}{\sqrt{2}\sigma} \right]}{1 + \text{Erf} \left[ \frac{\hat{\mu}}{\sqrt{2}\sigma} \right]} = 0.95/2 \quad (14)$$

---

<sup>4</sup> This neglects correlations and is therefore a rough approximation that should be taken with due caution. An estimate of the accuracy of this procedure can be done by comparing quantities derived from such combinations vs. the experimental ones, which typically agree within 5-10 %.



and

$$\int_{\hat{\mu}}^{\mu_{upL}} \text{PDF}(\mu) d\mu = \frac{\text{Erf} \left[ \frac{\hat{\mu}_{upL} - \mu}{\sqrt{2}\sigma} \right]}{1 + \text{Erf} \left[ \frac{\hat{\mu}}{\sqrt{2}\sigma} \right]} = 0.95/2. \quad (15)$$

However, when  $\hat{\mu} - \delta_{95}\hat{\mu} < 0$ , we shift the 95% C.L. interval to the asymmetric one  $(0, \mu_{upL})$  and revert to the upper limit definition [2, 13]<sup>5</sup>

$$\int_0^{\mu_{upL}} \text{PDF}(\mu) d\mu = \frac{\text{Erf} \left[ \frac{\hat{\mu}}{\sqrt{2}\sigma} \right] - \text{Erf} \left[ \frac{\hat{\mu} - \mu_{upL}}{\sqrt{2}\sigma} \right]}{1 + \text{Erf} \left[ \frac{\hat{\mu}}{\sqrt{2}\sigma} \right]} = 0.95. \quad (16)$$

To summarize, we cannot only exclude (at 95 % C.L.) a given scenario if it predicts too many signal events which are not seen ( $\mu > \mu_{upL}$ ), but also if it predicts too few events, incompatible with the observed excesses associated with reported discovery. The significance of such lower bounds will grow with more luminosity. Significances above  $5\sigma$  become possible (by definition) after discovery (which excludes the background hypothesis  $\mu = 0$ ). We will plot both of these bounds mapping the allowed  $\mu_{upL}^i, \mu_{dwL}^i$  into the relevant parameter space through the dependence of  $\mu_i$  on the free parameters in our fit results. In section V, figure 6, we give examples of such lower limits.

## B. Electroweak Precision Data

We incorporate EWPD [44–46] by adding it directly to the  $\chi^2$  measure in Eqn. (10). When  $a$  is considered a free parameter, the shifts of the oblique parameters S and T are given by [31]

$$\Delta S \approx \frac{-(1 - a^2)}{6\pi} \log \left( \frac{m_h}{\Lambda} \right), \quad \Delta T \approx \frac{3(1 - a^2)}{8\pi \cos^2 \theta_W} \log \left( \frac{m_h}{\Lambda} \right). \quad (17)$$

The numerical coefficient is determined from the logarithmic large- $m_h$  dependence of S, T given in Ref. [45].<sup>6</sup> As for EWPD, recent updates to the measurement of  $m_W$  at the Tevatron [47, 48] have refined the world average [49], and have significantly reduced the quoted error. Incorporating<sup>7</sup>

<sup>5</sup> The 95% C.L. interval extends down to 0 when the ratio  $\sigma/\hat{\mu} > 0.6$ , in which case there is no lower limit on  $\mu$  and the upper limit is given by Eqn. (16).

<sup>6</sup> Here we have introduced a Euclidean momentum cut-off scale  $\Lambda$ . The degree to which  $\Lambda$  properly captures the UV regularization of the S and T is model-dependent. We assume that directly treating this cut-off scale as a proxy for a heavy mass scale integrated out is a good approximation, i.e. that further arbitrary parameters rescaling the cut-off scale terms need not be introduced.

<sup>7</sup> We thank J. Erler for kindly providing these EWPD results.

these new measurements we use [50]

$$S = 0.00 \pm 0.10, \quad T = 0.02 \pm 0.11, \quad U = 0.03 \pm 0.09, \quad (18)$$

while the matrix of correlation coefficients is given by

$$C = \begin{pmatrix} 1 & 0.89 & -0.55 \\ 0.89 & 1 & -0.80 \\ -0.55 & -0.80 & 1 \end{pmatrix}. \quad (19)$$

Here we have assumed  $m_h = 125 \text{ GeV}$ , as corrections for shifting these results by a few GeV are negligible. There is a strong preference for  $a \simeq 1$  in the global fit when EWPD is used, and the constraints on the scalar field can be directly associated with EWPD bounds. Note that the slight preference for  $a > 1$  in the best-fit region when EWPD is taken into account is subject to uncertainties in cut-off scale effects. Although the shift in the best fit point is of interest as a probe of possible new physics, we cannot clearly disentangle such a hint from cut-off scale effects.

## IV. FIT RESULTS

### A. Status of the Higgs hypothesis

The excess of events of  $\approx 5\sigma$  significance reported by ATLAS and CMS peaks, as a function of the scalar mass at slightly different values:  $126.5 \text{ GeV}$  for ATLAS and  $125 \text{ GeV}$  for CMS. This difference can be attributed at this stage of the search to statistical fluctuations in the data. Monte-Carlo studies [51] indicate that such effects can shift the observed maximum signal strength compared to the true signal strength maximum by  $\sim 2 - 3 \text{ GeV}$ . Due to this, a fit that combines data from different experiments at the same mass value might be biased and not necessarily better than using data at slightly different masses. As much more detailed data is available to us at the mass peaks, in our global fits we will use all available  $\mu_i$  taken at  $m_h = 125 \text{ GeV}$  for the CMS and the Tevatron (which has an  $\approx 3\sigma$  excess over a wider region of masses), and at  $m_h = 126.5 \text{ GeV}$  for ATLAS (see Fig. 7 in the Appendix).

In order to assess the degree of consistency of the data with the SM hypothesis we first consider the effective Lagrangian given by  $\mathcal{L}_{eff}$  and assume that higher dimensional operators are sufficiently suppressed so that  $c_\gamma, c_g$  can be neglected. We then perform a two-parameter  $\chi^2(a, c)$  fit and examine the  $\Delta\chi^2$  for the SM point  $(a, c) = (1, 1)$  compared with the best fit point. This

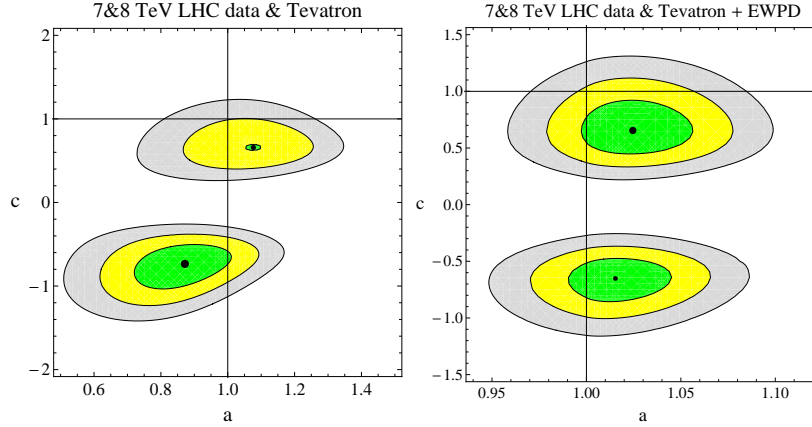


FIG. 1: Global fit results in the  $(a, c)$  plane for all reported best fit values given by ATLAS and CMS, left (right) without EWPD (with EWPD). In both plots we take  $m_h = 125$  GeV for the Tevatron and CMS7/8 and  $m_h = 126.5$  GeV for ATLAS7/8. The green, yellow, gray regions corresponds to the allowed 1, 2, 3  $\sigma$  spaces for a two parameter fit. The best fit point in each region is also labelled with a point.

defines a C.L. corresponding to the deviation of the SM hypothesis compared to the best fit point. The result is shown in Figure 1 (left). We also show in 1 (right) the best-fit regions when EWPD is added to the global  $\chi^2$  measure. Notice the dramatic reduction in the size of the best fit region along the  $a$ -parameter, which is forced to lie close to 1. These results visually summarize the current experimental status of establishing the Higgs hypothesis.

When EWPD is not used, the SM Higgs hypothesis of  $(a, c) = (1, 1)$  is  $\sim 2\sigma$  (C.L. of 0.95) away from the best fit point, which sits at  $(a, c) = (0.87, -0.74)$ . Note that here and in the following discussion we are choosing to round the C.L. and the best fit points. This is due to the preliminary nature of the 7 + 8 TeV data and is not limited directly to this accuracy due to the fit procedure we have adopted. The C.L. of the SM hypothesis in the combined data is consistent with our past results at 7 TeV [2]. Interestingly, the minimum in the fit space where  $c < 0$  is currently preferred. This is easy to understand due to the interference term in the  $h \rightarrow \gamma\gamma$  decay width which is  $\propto -ac$ . A negative  $c$  allows a relatively larger excess in  $\gamma\gamma$  events due to constructive interference between the top and  $W$  boson loops. When EWPD is used as in Figure 1 (right) we find that the SM is similarly residing at  $\sim 2\sigma$  (C.L. of 0.92) away from the best fit point which is now  $(a, c) = (1.0, 0.65)$  and the best-fit region where  $c > 0$  has a (slightly) lower global minimum. However, the minima are nearly degenerate with  $\Delta\chi^2(\min_1, \min_2) \lesssim 0.05$ .

In view of the different masses of the signal-strength peaks in the various experiments (which

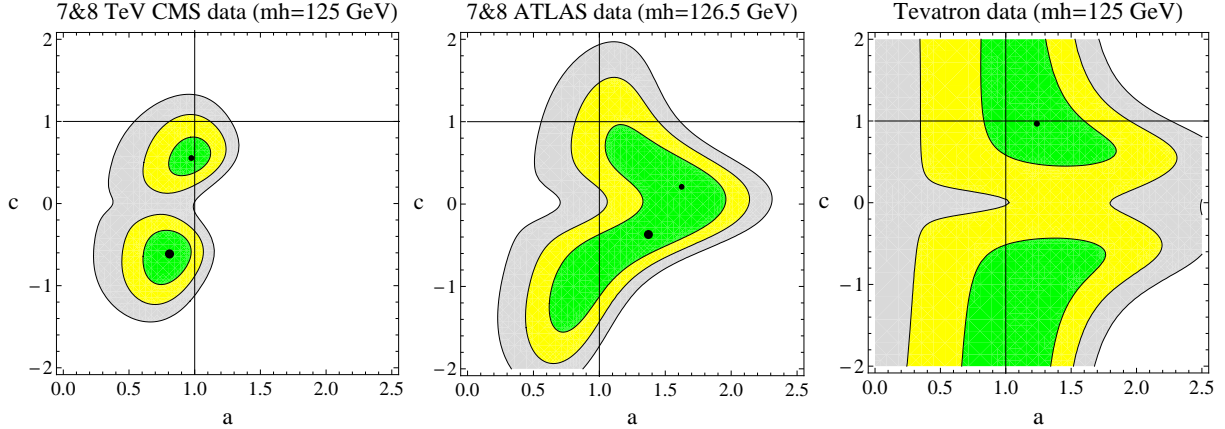


FIG. 2: Best-fit regions (at 68%, 95% and 99.9%) in the  $(a, c)$  plane for a fit to all reported signal-strength values given by ATLAS ( $m_h = 126.5$  GeV), CMS ( $m_h = 125$  GeV) and the Tevatron ( $m_h = 125$  GeV) collaborations individually. We plot the same best-fit contours over the same domain of parameter space to allow a direct comparison amongst experimental results.

can be due to the statistical effects mentioned above) and of the subtleties in properly combining the results of these different experiments we have neglected, it is also of interest to perform the fit in the  $(a, c)$  space for each experiment individually. We show these results in Figure 2. The LHC experiments have the SM point residing about  $\sim 2\sigma$  from the best fit point with the C.L. of the SM case compared to the best fit point at 81, 91% for ATLAS and CMS, respectively. The Tevatron results have the SM point within the  $1\sigma$  region with a C.L. of the SM case (compared to the best fit point) of 50%. The allowed fit region for CMS can be compared to the recently presented public results [1]. The morphology of the allowed fit regions is quite similar, however, the allowed fit space is significantly larger in the public CMS results. This is due to the fit method used. For example, the choice of only using the leading order results for  $h \rightarrow gg$  in the presented CMS result.

## B. BSM Implications

### 1. Implications for an invisible width

The results of the last section can be interpreted as (partial) evidence in support of the SM Higgs hypothesis. Assuming then that the observed boson is the SM Higgs, we can study possible deviations of its properties due to BSM effects. The simplest extension of the SM in terms of

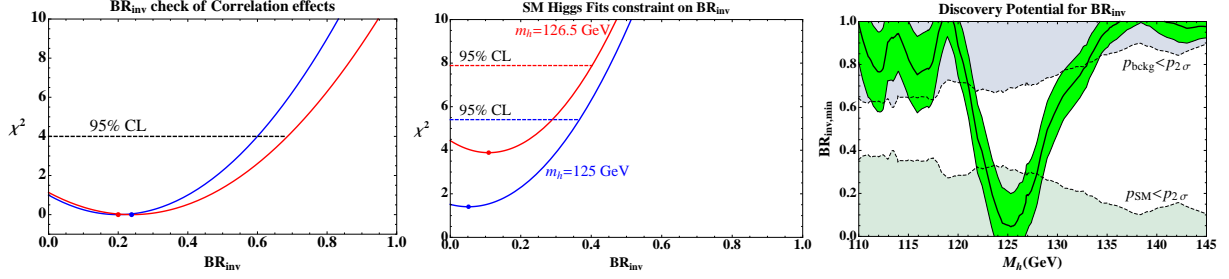


FIG. 3: Global fit to  $\text{Br}_{\text{inv}}$  for the SM Higgs using only CMS data (left) for  $m_h = 125$  GeV with two methods as a check of our fit procedure. See text for further explanation. The middle figure shows the  $\chi^2$  distribution developed from the combined best fit  $\hat{\mu}_c$  supplied by the four experiments, including the 7 and 8 TeV LHC results for two mass values. In the right figure we show the discovery potential for  $\text{Br}_{\text{inv}}$ , updating a result from the analysis in Ref. [38] with the new global signal strength data.

new parameters is perhaps the case where one only introduces a Higgs invisible branching ratio,  $\text{Br}_{\text{inv}}$ . Such an extension is common in many BSM scenarios, *e.g.* when new physics couples through the Higgs portal, and new states exist that are uncharged under the SM group. Fitting to  $\text{Br}_{\text{inv}}$  allows one to fit to the global combined signal strength values supplied by the experimental collaborations. The values we use to perform the fit are given in Table I.

Experiments	$\hat{\mu}_c, m_h = 125$	$\sigma_c, m_h = 125$	$\hat{\mu}_c, m_h = 126.5$	$\sigma_c, m_h = 126.5$
CMS [7&8 TeV] [1]	0.80	0.20	0.67	0.19
ATLAS [7&8 TeV] [1]	1.12	0.27	1.24	0.26
CDF&DØ [41]	1.35	0.59	1.38	0.60

TABLE I: Combined signal strengths  $\hat{\mu}_c$  and errors  $\sigma_c$  from ATLAS, CMS and the Tevatron collaborations. Here we quote  $\pm$  symmetric  $1\sigma$  errors.

The left plot of Fig.3 shows the result of extracting  $\text{Br}_{\text{inv}}$  using our fit approach in two different manners. This allows an important cross check of our result and procedure. We have employed two approximations that require further justification in our fit procedure. Using the assumption of Gaussian PDF's, we have extracted the 8 TeV data from the known 7 TeV data and the released 7 + 8 TeV data. In doing so we have neglected (unsupplied) correlations. Further in performing our fits we have neglected correlation coefficients for the  $\mu_i$ . Fitting to the combined CMS data directly - which do take into account correlations - and comparing the fit results to the case where we use our procedure to extract the 8 TeV data, and fit to the  $\mu_i$ , is shown in the left plot of

Fig.3. The best fit point and the 95% C.L. regions are in good agreement, supporting the estimated accuracy of our results of  $\sim 5 - 10\%$ .

The middle plot of Fig.3 shows the resulting  $\chi^2$  distributions for  $\text{Br}_{inv}$  for two different mass values  $m_h = 125, 126.5$  GeV. Here we combine the results from the four experiments and fit to the supplied signal strength parameters. We find the 95% C.L. regions are  $\text{Br}_{inv} < 0.37(40)$  for  $m_h = 125(126.5)$  GeV. These results are the most accurate extractions of the limit on  $\text{Br}_{inv}$  that we can perform with the released data and is more accurate than a fit on the individual channels. This is primarily due to the experimental correlation effects that are incorporated in the  $\hat{\mu}_c$ , and larger number of channels that are incorporated in the experimental likelihoods used to construct the combined signal strength parameter used.

The right plot of Fig.3 (which updates a similar analysis in Ref. [38]) shows the current status of the quantity  $(1 - \hat{\mu}_c)$  (with one sigma error band), interpreted as an invisible Higgs branching ratio, as a function of the Higgs mass. This result is also based on the combined signal strengths supplied by the experimental collaborations. With the current errors, no significant statement can be made about the possible nonzero value central value of  $\text{Br}_{inv}$ . The shaded areas indicate the  $2\text{-}\sigma$  range of possible fluctuations (of the background in the upper region at large  $\text{Br}_{inv}$ ; of the SM Higgs signal in the lower region at small  $\text{Br}_{inv}$ ) that could be miss-interpreted as an invisible Higgs width. The current nonzero central values of  $\text{Br}_{inv}$  at  $m_h \sim 125$  GeV (consistent with the fit results) are indicated by this plot to be perfectly compatible with downward fluctuations of the SM Higgs signal strength parameters.

## 2. Implications for $c_g, c_\gamma$

One can also infer the current experimental bounds on the BSM parameters  $c_g, c_\gamma$ . We expect that these operators arise at the loop level, so we rescale the Wilson coefficients as  $c_j = \tilde{c}_j/(16\pi^2)$  for  $j = g, \gamma$ . Using the results of Ref. [52], the effects of these operators are incorporated as rescaling factors used consistently in the fit given by

$$R_g \equiv \frac{\sigma_{gg \rightarrow h}}{\sigma_{gg \rightarrow h}^{SM}} \approx \left| 1 - \frac{1}{0.75c_t - (0.05 + 0.07i)c_b} \frac{v^2 \tilde{c}_g}{\Lambda^2} \right|^2, \quad (20)$$

$$R_\gamma \equiv \frac{\Gamma_{h \rightarrow \gamma\gamma}}{\Gamma_{h \rightarrow \gamma\gamma}^{SM}} \approx \left| 1 + \frac{1}{4(2.07a - 0.44c_t + (0.01 + 0.01i)c_b)} \frac{v^2 \tilde{c}_\gamma}{\Lambda^2} \right|^2. \quad (21)$$

Here we have used  $m_t = 172.5$  GeV,  $m_b = 4.75$  GeV,  $m_h = 125$  GeV and  $\alpha_s(172.5) = 0.107995$ . When the SM Higgs is assumed then  $a = c_t = c_b = 1$ . We have retained the two-loop QCD

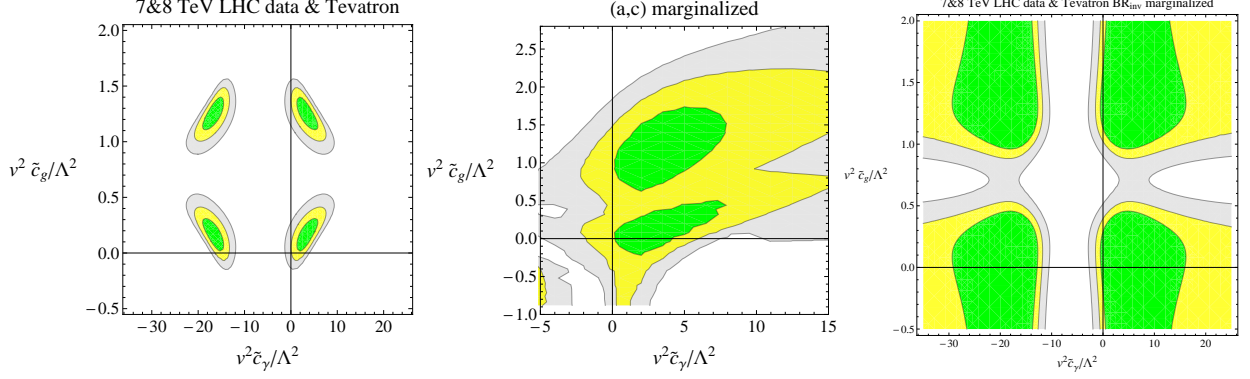


FIG. 4: (Left) Results of fitting to  $c_g, c_\gamma$  when the SM is assumed, (Middle): results of fitting to  $c_g, c_\gamma, a, c$  and marginalizing over (a,c) subject to the constraint  $a > 0$  and  $0 < c < 3$ , (Right):  $c_g, c_\gamma, \text{BR}_{inv}$  and the marginalizing over  $\text{BR}_{inv}$ .

correction to the SM matching of the  $h G_{\mu\nu}^A G^{A\mu\nu}$  operator in the  $m_t \rightarrow \infty$  limit in these numerical coefficients. The operators in  $\mathcal{L}_{HD}^5$  also affect  $\text{Br}(h \rightarrow \gamma Z)$ , but the effects in our fit can be neglected. See Ref. [38] for further details and discussion on our fitting procedure to these higher dimensional operators.

We show in Figure 4 the results of fitting to  $c_g, c_\gamma$  using the current dataset when one assumes the SM (left), when one fits to  $c_g, c_\gamma, a, c$  and subsequently marginalizes over  $a, c$  (middle) and finally when one fits to  $c_g, c_\gamma, \text{BR}_{inv}$  and marginalizing over  $\text{BR}_{inv}$ . These results summarize the preference in the current dataset for including higher dimensional operators when the scalar is not assumed to be the Higgs.

We also show the case where one fits to  $c_g, c_\gamma, a, c$  and marginalizes over the higher dimensional operators in Fig. 5 (left). This latter case shows the preference for  $a, c$  even when more massive states are integrated out of a composite scalar theory (for example) leading to  $c_g, c_\gamma$ . We see that the SM hypothesis is significantly improved in its consistency with the data set in the context of NP of this form. A final plot in Fig. 5 (right) shows the allowed space when  $c_t$  is varied independently from the remaining fermion couplings which are treated with a universal rescaling.

The fit to higher dimensional operators shows a preference for a BSM contribution to  $c_\gamma$ . The possibility of an enhancement of  $c_\gamma$  deserves some comment. First, one can study the model independence of the preference for an enhancement of  $c_\gamma$  by constructing a one dimensional  $\chi^2$  distribution, marginalizing over the unknown operator  $c_g$  when the SM is assumed, or over  $(c_g, a, c)$  when one is considering non-SM scalar scenarios. Performing this exercise we find that a pref-

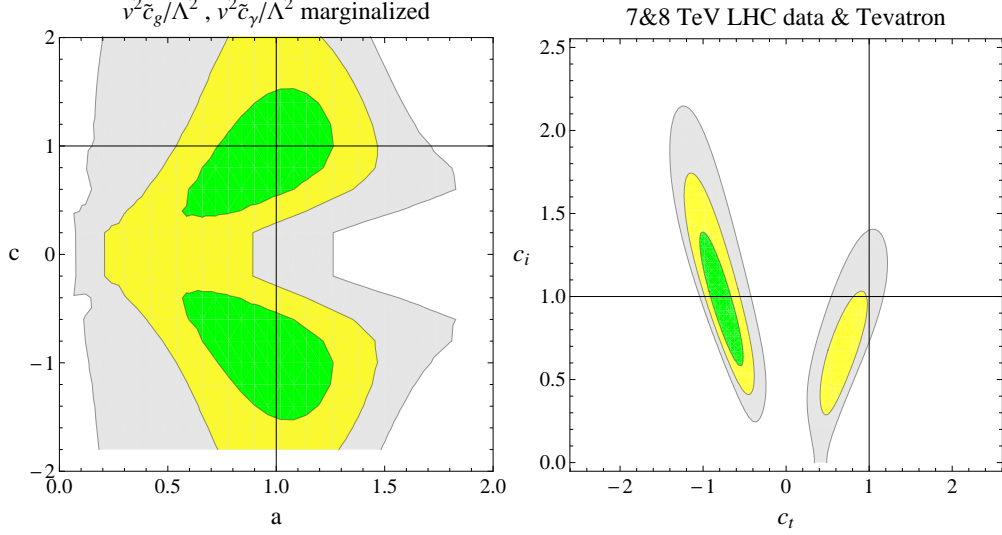


FIG. 5: Left plot: fit to  $c_g, c_\gamma, a, c$  and marginalizes over the higher dimensional operators, right plot: allowed space when  $c_t$  is varied independently. See text for more details.

ference for  $c_\gamma \neq 0$  only exists in certain cases where implicit UV assumptions are adopted due to the parameters used to fit the data. One can make a number of observations regarding enhanced  $h \rightarrow \gamma\gamma$  event rates. The coupling to  $F_{\mu\nu}$  can come about due to  $c_{WB}$ . If this is the case, one can bound the allowed enhancement of  $\mu_{\gamma\gamma}$  due to related EWP constraints. Using the relation [52–54]

$$\frac{v^2}{\Lambda^2} \tilde{c}_{WB} = -2\pi S, \quad (22)$$

one finds the current experimental constraint  $|\frac{v^2}{\Lambda^2} \tilde{c}_{WB}| \lesssim N 0.63$  for an  $N\sigma$  deviation considered in the EWP parameter  $S$ , assuming  $m_h = 125 \text{ GeV}$ . Using  $\mu_{\gamma\gamma} \approx R_g R_\gamma$ , this leads to the bound that  $\mu_{\gamma\gamma} < 1.2 (1.4)$  for a one (two) sigma deviation in the  $S$  parameter when  $c_g = 0$ . Restricting the unknown higher dimensional operators to have a global  $\chi^2$  measure in the  $2\sigma$  allowed region ( $\Delta\chi^2(c_g, c_\gamma) < 6.18$ ), one can maximize the enhancement of  $\mu_{\gamma\gamma}$  considering the related constraints on  $c_{WB}$ . One finds an enhancement of 3.2 is possible when a one sigma deviation in the  $S$  parameter is allowed. The  $c_\gamma$  Wilson coefficient could also come about due to  $c_B, c_W$  or a combination of these Wilson coefficients. In this case, the EWP constraint does not directly apply, and an enhancement of  $\mu_{\gamma\gamma}$  by a factor of  $\lesssim 3.5$  is still allowed when maximizing the contribution subject to the constraint that the  $\Delta\chi^2(c_g, c_\gamma) < 2.3$ .

This analysis has assumed no relationship between the Wilson coefficients  $c_\gamma, c_g$ , which is fixed in any particular underlying model matched onto. It is interesting to note that in general



when matching onto a single BSM field one expects a strong relationship between the Wilson coefficients. With identical loop functions in many cases, and the only differences in the matching onto the Wilson coefficients coming about due to the relative charges of the new states under the SM subgroups  $SU(3)$  and  $U(1)_{\text{em}}$ .

## V. STUDIES OF CONSISTENCY AND TENSION WITHIN THE DATA SET

The consistency between the search results  $(\hat{\mu}_i \pm \sigma_i)$  from different channels can be quantified as follows. For each channel  $i$  we construct its Gaussian approximation to the pdf of the signal strength,  $p_i(\mu) = pdf(\mu, \hat{\mu}_i, \sigma_i)$ , which we can contrast with the full combined PDF (either in a given experiment or for the overall combination of all data). For each single channel we calculate its  $p$ -value with respect to the global  $PDF(\mu) = pdf(\mu, \hat{\mu}_c, \sigma_c)$ , *i.e.*,  $p_i$  is the  $p$ -value for  $\hat{\mu}_i$  assuming the full  $PDF(\mu)$ :

$$\begin{aligned} p_i &\equiv \int_0^{\hat{\mu}_i} PDF(\mu) d\mu \quad (\hat{\mu}_i < \hat{\mu}_c) , \\ p_i &\equiv 1 - \int_{\hat{\mu}_i}^{\infty} PDF(\mu) d\mu , \quad (\hat{\mu}_i > \hat{\mu}_c) . \end{aligned} \quad (23)$$

We will say channel  $i$  is in tension with the rest of the data if  $p_i$  is very small. For a given critical  $p$ -value  $p_c$ , channel  $i$  is not consistent with the combined dataset at  $(1 - p_c)$  C.L. if  $p_i < p_c$  and the model can be excluded based on that disagreement. For concreteness we will chose  $p_c = 10^{-3}$  (*i.e.* 99.9% C.L.).

When this test for consistence is applied to the  $(\hat{\mu}_i \pm \sigma_i)$  dataset, interpreted as coming from a SM Higgs signal, we find no tension at this level for any channel. However, in extensions of the SM, like the two-parameter scenario  $SM(a, c)$  we have discussed in previous sections, the rescaling of the different channels can introduce very significant distortions in the pdfs and cause too large tensions for some channels. Such regions of parameter space can therefore be excluded on this basis. Figure 6 illustrates this by showing the regions in  $(a, c)$  space that would be excluded due to such inconsistency in some search channel (regions delimited by the blue lines). We show both the limits experiment by experiment and the combined result. Typically, in the excluded regions several channels at the same time cause the exclusion. We show in each case all the region that is excluded by at least one channel. In each case, the channels that have bigger exclusion-power are the following. For Tevatron, the  $b\bar{b}$  and  $\gamma\gamma$  channels; for CMS,  $\gamma\gamma jj$  and  $\tau\tau$ ; for ATLAS,  $\gamma\gamma$ ,  $ZZ$  and  $\tau\tau$ ; while for the combined dataset, the most powerful channels are  $\gamma\gamma jj$  and  $b\bar{b}$ . We

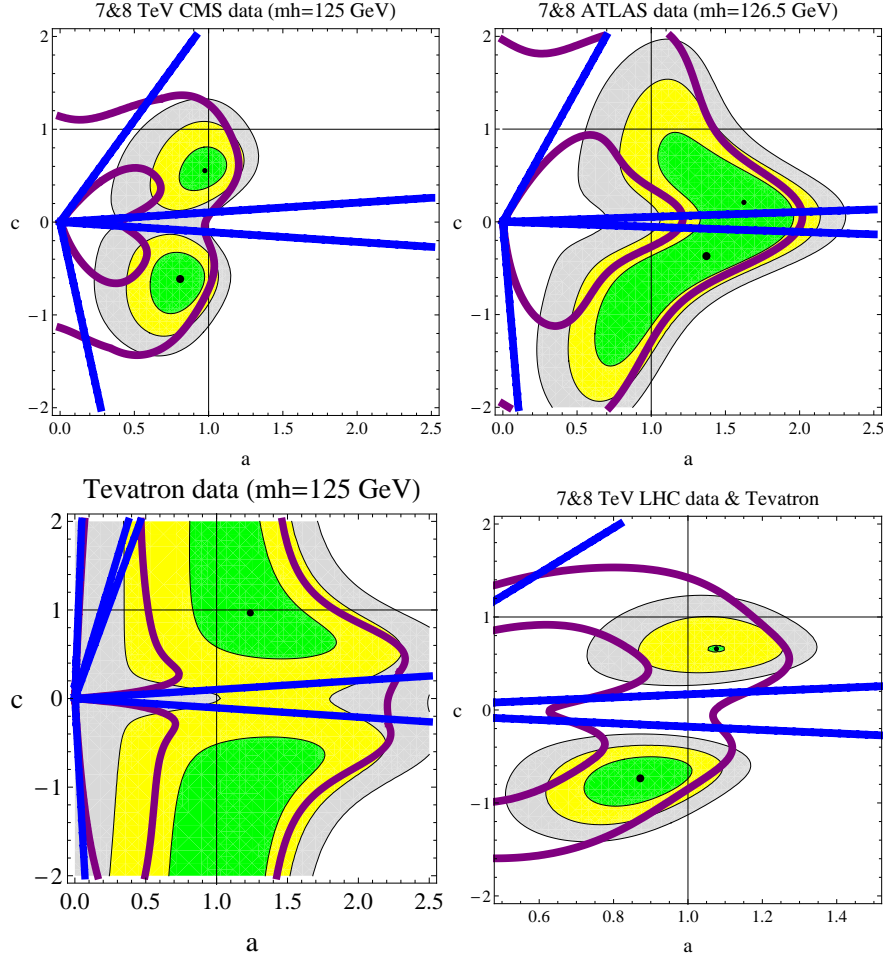


FIG. 6: Exclusion limits on the  $SM(a, c)$  parameter space derived from a) 95% C.L. upper limits on the signal strength parameter  $\hat{\mu} < \mu_{upL}$  (solid purple lines towards the right), b) 95% C.L. lower limits  $\hat{\mu} > \mu_{dwL}$  (solid purple lines close to the origin) and c) "tension limits" (dashed purple lines) from the presence of search channels inconsistent with the rest of the dataset at 99.9% C.L. (the most powerful channels in setting such limits are indicated in parentheses below, for each case). Upper left: CMS-only data ( $\gamma\gamma jj$  and  $\tau\tau$ ). Upper right: ATLAS-only data ( $\gamma\gamma$ ,  $ZZ$  and  $\tau\tau$ ). Lower left: Tevatron-only data ( $b\bar{b}$  and  $\gamma\gamma$ ). Lower right: Full combined dataset ( $\gamma\gamma jj$  and  $b\bar{b}$ ). For comparison, the best-fit regions discussed in previous sections are also shown. The excluded regions can be readily identified by knowing that the best fit points are not excluded. The fermiophobic scenario along  $c = 0$  is excluded.

see from Figure 6, that fermiophobic scenarios, along the axis  $c = 0$ , are excluded at this level of confidence.

This channel-tension analysis is clearly related to the  $\chi^2$  study we have also performed and the tension exclusion limits tend to exclude regions of parameter space that give a bad fit to the

data. However, this approach seems to be more powerful in being able to exclude definitely some models. We also see that there are regions of parameter space that are not excluded by the conventional upper (or lower) limits imposed on the signal strength parameter, yet can be excluded by the tension exclusion-limit. This is simply due to the fact that the dataset can contain two widely separate channels and still give a combined PDF that respects the upper limit, which is not able to probe in such cases the internal inconsistency of the individual channels. We conclude that this type of analysis offers a complementary tool in testing model performance.

## VI. CONCLUSIONS.

We have studied the evidence of a scalar field that has been reported discovered by the LHC collaborations using an effective field theory framework. We have discerned what can be inferred about the properties of the scalar field at this time using joint  $\chi^2$  fits to available data sets. We have also developed and applied new techniques that allow one to exclude model classes that are in tension with the data through violating upper or lower CL bounds, or through introducing excessive tension into the signal strength parameter data sets. At this time, according to our fit method, and using publicly available data, the SM Higgs hypothesis is consistent with the global data set at the level of  $2\sigma$ .

## Appendix A: Data Used

Our approach to the presented data is as follows. As the effect of reweighing the various contributions to the inclusive Higgs production processes depends on the operating energy of LHC, we require a method to fit to 7 and 8 TeV data separately. It is not sufficient to use the expected fraction of events for each operating energy and integrated luminosity in the SM to reweigh the Higgs signal strengths and directly fit 7, 8 TeV signal strengths. This would introduce a further bias in the fit as the relative fraction of events at each operating energy depends on the unknown parameters  $a, c, c_g, c_\gamma$ . The recently presented results [1] have only a subclass of the data presented separated in 7, 8 TeV signal strengths. When 7 and 8 TeV data is presented separately, we directly use this data.

However, we note that using the approximation of gaussian PDF's describing the data (which is increasingly accurate as the total number of events increases) and dictating the signal strengths,

one can use the results of Eqn. 12 to reconstruct the unreported 8 TeV data in the channels where only 7 + 8 and 7 TeV signal strengths have been supplied. This can be done without knowing directly the experimental likelihood function in the limit that correlations are neglected, which is an assumption we are already forced to adopt as this information is not supplied by the experimental collaborations. We show in Fig. 7 the resulting reconstructed data. Clearly it is preferable to have directly the experimental signal strengths for 8 TeV alone to perform this fit, we will update our results when such information is released.

An interesting check of our approach is to use a subset of the provided subclass signal strengths to reproduce a reported combined signal strength. This exercise can be carried out, for example, on the supplied vector boson fusion tagging  $b\bar{b}$  signal strength and  $t\bar{t}h$  signal strength (that uses  $h \rightarrow b\bar{b}$ ) and comparing to the presented combined  $h \rightarrow b\bar{b}$  signal strength. We have carried out this procedure for the presented CMS data and find good agreement with the reported results, within our estimate of 5 – 10% error introduced due to a lack of correlations.

For the  $pp \rightarrow \gamma\gamma jj$  signals of CMS have gluon contaminations due to  $gg$  Higgs production events, so that the relevant signal rate is given by

$$(\epsilon \sigma_{gg \rightarrow h} + \sigma_{jjh}) \times \text{Br}(h \rightarrow \gamma\gamma). \quad (\text{A1})$$

We use  $\epsilon = 0.32$  for the 7 TeV dijet tagged di-photon signal,  $\epsilon = 0.23$  for the 8 TeV “tight” dijet tagged diphoton data and  $\epsilon = 0.39$  for the 8 TeV “loose” dijet tagged diphoton data [55]. We thank V. Sanz for kindly providing these contamination coefficients.

### Acknowledgments

We thank A. Djouadi, J. Erler, B. Feigl, R. Gonalo, R. Harlander, A. Juste, M. Martinez, M. Schumacher, M. Spira, W. Fisher, J. Huston, V. Sanz, V. Sharma, P. Uwer, J. Bendavid and A. Delgado for helpful communication on related theory and data. This work has been partly supported by the European Commission under the contract ERC advanced grant 226371 MassTeV, the contract PITN-GA-2009-237920 UNILHC, and the contract MRTN-CT-2006-035863 ForcesUniverse, as well as by the Spanish Consolider Ingenio 2010 Programme CPAN (CSD2007-00042) and the Spanish Ministry MICNN under contract FPA2010-17747 and FPA2008-01430. MM is supported by the DFG SFB/TR9 Computational Particle Physics. Preprints: KA-TP-29-2012,

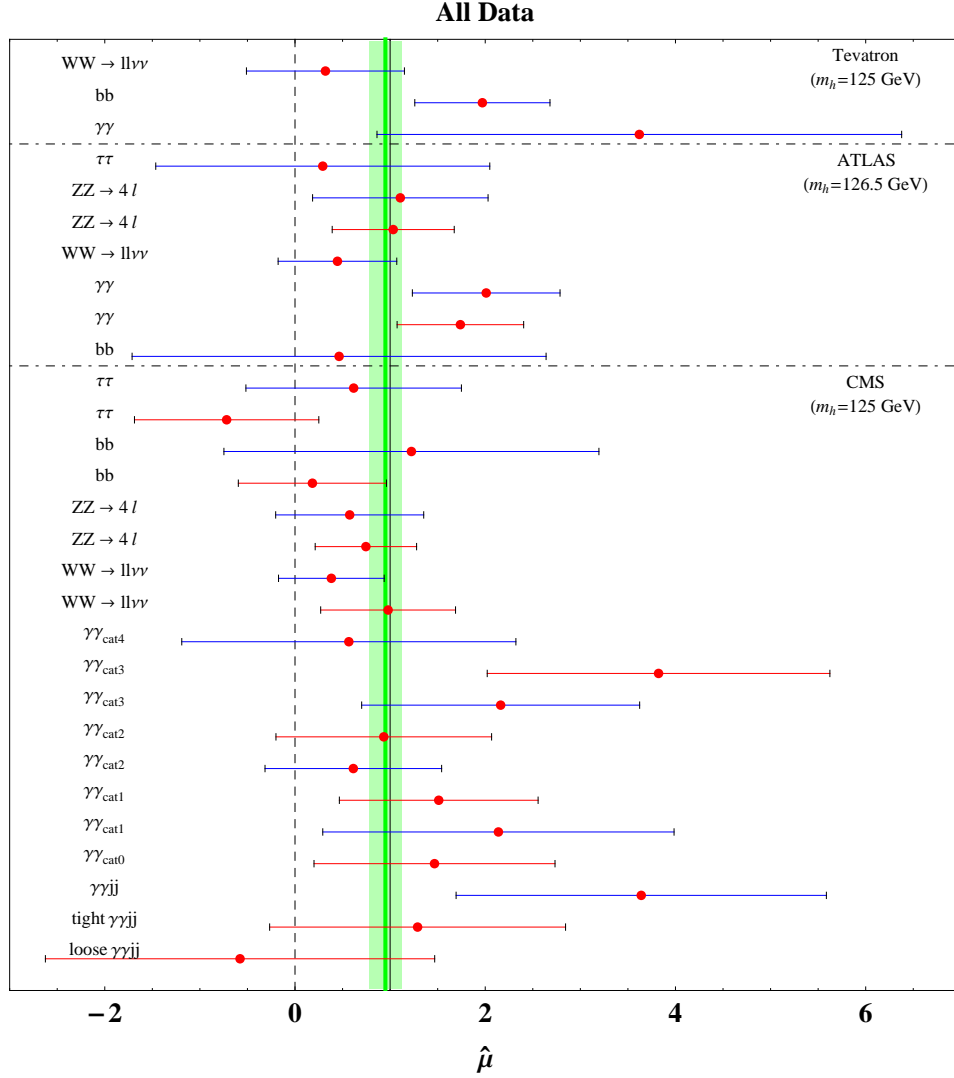


FIG. 7: Pictorial presentation of the data used in the fits to sub-channels, Blue bands reported data at 7 TeV. Red, reported 8 TeV data, or reconstructed 8 TeV data.

SFB/CPP-12-48, CERN-PH-TH/2012-151. Ref. [56–58] appeared as this draft was completed.

- 
- [1] ATLAS and CMS collaborations, Wed July 4th, CERN.
  - [2] J. R. Espinosa, C. Grojean, M. Muhlleitner and M. Trott, JHEP **1205** (2012) 097 [arXiv:1202.3697 [hep-ph]].
  - [3] R. S. Chivukula and H. Georgi, Phys. Lett. B **188** (1987) 99.
  - [4] L. J. Hall and L. Randall, Phys. Rev. Lett. **65**, 2939 (1990).

- [5] G. D'Ambrosio, G. F. Giudice, G. Isidori and A. Strumia, Nucl. Phys. B **645** (2002) 155 [arXiv:hep-ph/0207036].
- [6] A. J. Buras, Acta Phys. Polon. B **34**, 5615 (2003) [arXiv:hep-ph/0310208].
- [7] V. Cirigliano, B. Grinstein, G. Isidori and M. B. Wise, Nucl. Phys. B **728** (2005) 121 [arXiv:hep-ph/0507001].
- [8] M. A. Shifman *et al.* Sov. J. Nucl. Phys. **30**, 711 (1979) [Yad. Fiz. **30**, 1368 (1979)].
- [9] A. I. Vainshtein *et al.* Sov. Phys. Usp. **23**, 429 (1980) [Usp. Fiz. Nauk **131**, 537 (1980)].
- [10] L. Susskind, Phys. Rev. D **20** (1979) 2619.
- [11] S. Weinberg, Phys. Rev. D **19** (1979) 1277.
- [12] P. Sikivie *et al.* Nucl. Phys. B **173** (1980) 189.
- [13] A. Azatov, R. Contino and J. Galloway, JHEP **1204** (2012) 127 [hep-ph/1202.3415].
- [14] D. Carmi, A. Falkowski, E. Kuflik and T. Volansky, [hep-ph/1202.3144].
- [15] P. P. Giardino, K. Kannike, M. Raidal and A. Strumia, JHEP **1206** (2012) 117 [arXiv:1203.4254 [hep-ph]]; [hep-ph/1207.1347].
- [16] J. Ellis and T. You, JHEP **1206** (2012) 140 [arXiv:1204.0464 [hep-ph]].
- [17] R. Lafaye *et al.* JHEP **0908**, 009 (2009) [hep-ph/0904.3866].
- [18] C. Englert *et al.* Phys. Lett. B **707**, 512 (2012) [hep-ph/1112.3007].
- [19] M. Klute *et al.* [hep-ph/1205.2699].
- [20] T. Corbett, O. J. P. Eboli, J. Gonzalez-Fraile, M. C. Gonzalez-Garcia, [hep-ph/1207.1344].
- [21] D. Carmi, A. Falkowski, E. Kuflik and T. Volansky, arXiv:1206.4201 [hep-ph].
- [22] A. Azatov, R. Contino and J. Galloway, arXiv:1206.3171 [hep-ph].
- [23] G. F. Giudice, C. Grojean, A. Pomarol and R. Rattazzi, JHEP **0706**, 045 (2007) [hep-ph/0703164].
- [24] R. Contino *et al.* JHEP **1005**, 089 (2010) [hep-ph/1002.1011].
- [25] R. Grober and M. Muhlleitner, JHEP **1106**, 020 (2011) [hep-ph/1012.1562].
- [26] M. Bando, K. -i. Matumoto and K. Yamawaki, Phys. Lett. B **178**, 308 (1986).
- [27] W. D. Goldberger, B. Grinstein and W. Skiba, Phys. Rev. Lett. **100**, 111802 (2008) [arXiv:0708.1463 [hep-ph]].
- [28] D. B. Kaplan and H. Georgi, Phys. Lett. B **136**, 183 (1984).
- [29] D. B. Kaplan, H. Georgi and S. Dimopoulos, Phys. Lett. B **136**, 187 (1984).
- [30] K. Agashe, R. Contino and A. Pomarol, Nucl. Phys. B **719**, 165 (2005) [hep-ph/0412089].
- [31] R. Barbieri, B. Bellazzini, V. S. Rychkov and A. Varagnolo, Phys. Rev. D **76**, 115008 (2007)

- [arXiv:0706.0432 [hep-ph]].
- [32] M. Farina, C. Grojean and E. Salvioni, arXiv:1205.0011 [hep-ph].
- [33] R. Schabinger and J. D. Wells, Phys. Rev. D **72**, 093007 (2005) [hep-ph/0509209].
- [34] B. Patt and F. Wilczek, hep-ph/0605188.
- [35] J. March-Russell *et al.* JHEP **0807**, 058 (2008) [hep-ph/0801.3440].
- [36] J. R. Espinosa and M. Quiros, Phys. Rev. D **76**, 076004 (2007) [hep-ph/0701145].
- [37] M. Pospelov and A. Ritz, Phys. Rev. D **84**, 113001 (2011) [arXiv:1109.4872 [hep-ph]].
- [38] J. R. Espinosa, M. Muhlleitner, C. Grojean and M. Trott, arXiv:1205.6790 [hep-ph].
- [39] G. Aad *et al.* [ATLAS Collaboration], arXiv:1207.0319 [hep-ex].
- [40] S. Chatrchyan *et al.* [CMS Collaboration], Phys. Lett. B **710**, 26 (2012) [arXiv:1202.1488 [hep-ex]].
- [41] Tevatron New Pheno. Higgs WG, [http://tevnpnphwg.fnal.gov/results/SM\\_Higgs\\_Summer\\_12/index.html](http://tevnpnphwg.fnal.gov/results/SM_Higgs_Summer_12/index.html)
- [42] S. Dittmaier *et al.* [LHC Higgs Cross Section WGC], [hep-ph/1101.0593].
- [43] A. Djouadi, J. Kalinowski and M. Spira, Comput. Phys. Commun. **108**, 56 (1998) [hep-ph/9704448].  
A. Djouadi, J. Kalinowski, M. Muhlleitner and M. Spira in J.M. Butterworth *et al.*, arXiv:1003.1643 [hep-ph].
- [44] B. Holdom and J. Terning, Phys. Lett. B **247** (1990) 88. M. E. Peskin and T. Takeuchi, Phys. Rev. Lett. **65** (1990) 964. M. Golden and L. Randall, Nucl. Phys. B **361** (1991) 3.
- [45] M. E. Peskin and T. Takeuchi, Phys. Rev. D **46** (1992) 381.
- [46] G. Altarelli and R. Barbieri, Phys. Lett. B **253** (1991) 161. G. Altarelli, R. Barbieri and S. Jadach, Nucl. Phys. B **369** (1992) 3 [Erratum-ibid. B **376** (1992) 444].
- [47] T. Aaltonen *et al.* [CDF], Phys. Rev. Lett. **108**, 151803 (2012) [arXiv:1203.0275 [hep-ex]].
- [48] V. M. Abazov *et al.* [D0], Phys. Rev. Lett. **108**, 151804 (2012) [arXiv:1203.0293 [hep-ex]].
- [49] Tevatron Electroweak WG, f. t. C. Coll. and D. Coll., arXiv:1204.0042 [hep-ex].
- [50] J. Erler, Private communication.
- [51] B. Murray, RAL Higgs Workshop 28th March 2012, <http://indico.cern.ch/getFile.py/access?contribId=84&sessionId=18&resId=0&materialId=slides&confId=162621>
- [52] A. V. Manohar and M. B. Wise, Phys. Lett. B **636**, 107 (2006) [hep-ph/0601212].
- [53] Z. Han and W. Skiba, Phys. Rev. D **71**, 075009 (2005) [hep-ph/0412166].
- [54] B. Grinstein and M. B. Wise, Phys. Lett. B **265**, 326 (1991).

- [55] J.R. Espinosa, C. Grojean, V. Sanz and M.Trott, In preparation.
- [56] P. P. Giardino, K. Kannike, M. Raidal and A. Strumia, arXiv:1207.1347 [hep-ph].
- [57] I. Low, J. Lykken and G. Shaughnessy, arXiv:1207.1093 [hep-ph].
- [58] T. Corbett, O. J. P. Eboli, J. Gonzalez-Fraile and M. C. Gonzalez-Garcia, arXiv:1207.1344 [hep-ph].